Title: Selection for early reproduction leads to accelerated aging and extensive metabolic remodeling in *Drosophila melanogaster*

Authors: David L. Hubert[1*], Kenneth R. Arnold[2], Zachary G. Greenspan[2], Anastasia Pupo[2], Ryan D. Robinson[2], Valeria V. Chavarin[2], Thomas B. Barter[3], Danijel Djukovic[4], Daniel Raftery[4], Zer Vue[5], Antentor Hinton Jr.[5], Melanie R. McReynolds[6], Benjamin R. Harrison[7], and Mark A. Phillips[1*]

[1]Department of Integrative Biology, Oregon State University

[2]Department of Ecology and Evolutionary Biology, University of California, Irvine

[3]Children's Hospital Los Angeles

[4]Northwest Metabolomics Research Center, Department of Anesthesiology and Pain Medicine, University of Washington

[5] Department of Molecular Physiology and Biophysics, Vanderbilt University, Nashville, TN, 37232, USA.

[6]Department of Biochemistry and Molecular Biology, The Huck Institutes of the Life Sciences Pennsylvania State University, University Park, PA 16802

[7]Department of Lab Medicine and Pathology, University of Washington

[*]Corresponding authors: David Hubert (david.hubert@oregonstate.edu) and Mark Phillips (philmark@oregonstate.edu)

Abstract

Experimental evolution studies that feature selection on life-history characters are a proven approach for studying the evolution of aging and variation in rates of senescence. Recently, the incorporation of genomic and transcriptomic approaches into this framework has led to the identification of hundreds of genes associated with different aging patterns. However, our understanding of the specific molecular mechanisms underlying these aging patterns remains limited. Here, we incorporated extensive metabolomic profiling into this framework to generate mechanistic insights into aging patterns in *Drosophila melanogaster*. Specifically, we characterized metabolomic change over adult lifespan in populations of *D. melanogaster* where selection for early reproduction has led to an accelerated aging phenotype relative to their controls. Using these data we: i) evaluated evolutionary repeatability across the metabolome; ii) assessed the value of the metabolome as a predictor of “biological age” in this system; and iii) identified specific metabolites associated with accelerated aging. Generally, our findings suggest that selection for early reproduction resulted in highly repeatable alterations to the metabolome and the metabolome itself is a reliable predictor of “biological age”. Specifically, we find clusters of metabolites that are associated with the different rates of senescence observed between our accelerated aging population and their controls, adding new insights into the metabolites that may be driving the accelerated aging phenotype.

Significance

While experimental evolution studies featuring *Drosophila melanogaster* have generated significant insights into the forces that shape aging and life history patterns, more recent efforts incorporating genomic and transcriptomic data have had comparatively little success identifying the molecular mechanisms underlying these patterns. Here we work to incorporate molecular phenotyping into this general framework as a way forward. Specifically, we characterize how the metabolome changes with age in populations of *D. melanogaster* where hundreds of generations of selection for early reproduction have led to enrichment for an accelerated aging phenotype. By comparing to control populations, we show that the metabolome does appear to capture true signals of “biological age” and provides a new avenue for understanding the factors that underlie complex trait variation in real populations.

Introduction

Experimental evolution studies using *Drosophila melanogaster* populations have been a continual source of insight into the factors that underlie differences in longevity and rates of senescence between individuals. As predicted by the evolutionary theory of aging, selection for early reproduction reliably produces populations enriched for individuals that develop quickly and die young, whereas selection for postponed reproduction has the opposite effect (Rose 1984; Luckinbill et al. 1984; Chippindale 1997; Rose et al. 2010). Studying these populations has in turn generated many novel insights into the physiological trade-offs associated with different rates of senescence. For instance, while populations selected for early reproduction develop quickly and have high early life fecundity, they also exhibit reductions in egg viability (Chippindale et al. 1997), stress resistance (Kezos et al. 2023), lifetime fecundity, and lifespan (Burke et al. 2016). The goal of the current project is to build on this work to better understand the molecular underpinnings of this “accelerated aging” phenotype.

Over the past decade, the combination of experimental evolution and next-generation sequencing technologies has emerged as a powerful tool for studying the genetics of complex traits. Major findings from studies that analyze quantitative traits, such as longevity, stress resistance, and body size, have consistently shown that the underlying genetic architecture is complex, often involving hundreds of genes (e.g. Burke et al. 2010; Turner et al. 2011; Fabian et al. 2018; Tobler et al. 2015; Barter et al. 2019; Kezos et al. 2019). Studies have also found that many of these traits may involve genes with significant pleiotropic interactions (Greenspan et al. 2024), and suggest genetic redundancy is a common feature of complex trait genetic architecture (Hardy et al. 2018; Barghi et al. 2019). Because of this inherent complexity, direct insights into the molecular mechanisms underlying trait variation have been modest. With respect to aging and longevity, functional conclusions are largely limited to enrichment for gene ontology terms broadly related to neurological development, immune function, and metabolism (Carnes et al. 2015; Fabian et al. 2018, Barter et al. 2019). In an effort to move beyond the finding that complex traits are highly polygenic, some have turned to metabolomics as a path forward (e.g. Phillips et al. 2022; Cavigliasso et al. 2023).

Metabolomics involves the profiling of metabolites, molecules <2000 Da, collectively referred to as the metabolome. Because metabolites constitute the functional and energetic building blocks of all life, metabolomics provides a potential link between genotype and phenotype (Harrison et al. 2020). Among the -omic layers of systems biology (e.g. transcriptome, proteome, etc.) the metabolome is thought to closely reflect organismal phenotypes (Dettmer et al. 2007;

Hoffman et al. 2014). While genomic, transcriptomic, and proteomic signals can be complicated by epigenetic and posttranslational modifications, it is thought that the downstream positionality of the metabolome provides a marker more representative of the observed phenotype (Patti et al. 2012). The metabolome of flies is highly dynamic with age and is sensitive to effects on longevity from environmental conditions, genetic variation, and pharmacological interventions (Avanesov et al. 2014; Laye et al. 2015; Jin et al. 2020).

With respect to characterizing age sensitive effects, Zhao et al. (2022) recently used metabolomic data to build a multivariate age-prediction model colloquially referred to as a "metabolomic clock". As with other -omic clocks such as epigenetic clocks, the age prediction is not fully accurate (Rutledge et al. 2022; Parrott and Bertucci 2019). Indeed, the deviation of the age prediction from the fly metabolome clock from chronological age of the sampled flies, the flies so-called 'age acceleration', correlated with mortality rate and the remaining life expectancy of isogenic flies (Zhao et al., 2022). That is, fly strains whose predicted age was younger than their chronological age tended to live longer than flies whose predicted age was greater than their chronological age. Thus, the metabolome clock connects patterns of age in the metabolome to the rise in mortality risk that defines biological aging. Using clock models could provide insight into the molecules associated with the relative pace of chronological and biological age, where the former is simply a measure of the passing of time, and the latter is a relative measure of senescence (Jylhävä et al. 2017). In an experimental evolution context, such clock models could allow us to test hypotheses about the aging patterns that result from selection on life history (Parrott and Bertucci 2019).

Here, we applied metabolomic analysis to a set of ten replicate fruit fly populations where hundreds of generations of selection for early reproduction (Figure 1) has led to enrichment for an accelerated aging phenotype where flies develop quickly and die young relative to controls. In effect, creating a disconnect between the chronological and biological age when compared to the ancestral population. Previous work in this system has consistently demonstrated the evolutionary repeatability of this accelerated aging signal with high levels of genomic (Graves et al. 2017), transcriptomic, (Barter et al. 2019), and phenotypic convergence (Burke et al. 2016; Kezos et al. 2023) between newly derived and long-standing populations subjected to the same selection regime. This rapid convergence has been attributed to the hypothesis that adaptation in these populations is primarily fueled by shifts in common genetic variants present in the ancestral population that this system was derived from.

In Phillips et al. (2022), we compared metabolomic differentiation patterns between samples of 21-day-old flies from the accelerated aging (A-type) populations and their controls (C-type) and found evidence of altered tricarboxylic acid (TCA) cycle activity, carbohydrate metabolism, and neurological function in the A-type populations. Because age-specific mortality rates are known to greatly diverge between the fly populations by day 21, we concluded that the observed differences in metabolic activity were a potential driver of the aging and longevity differences observed between the selection regimes. One possibility is that these differences were due to metabolic remodeling, similar to the differences between reproductive and non-reproductive flies (Koliada et al. 2020; Rodrigues et al. 2023). Such remodeling in the A-type populations could meet energetic and nutritional demands associated with fast development and early reproduction and come at the expense of somatic maintenance. However, our ability to make a definitive statement was limited as Phillips et al. (2022) included only a single age class and did not establish if this metabolomic difference reflected a difference in biological aging. In the present study, we seek to remedy this shortcoming and derive even deeper mechanistic insights by testing for accelerated biological age and characterizing how metabolomic profiles change over time in the A and C-type regimes by sampling at multiple age classes (Figure 2).

We hypothesize that the metabolome is connected to the physiological tradeoffs that accompany adaptation to the A-type selection regime. If true, we predicted that i) metabolomic profiles should rapidly converge for populations subjected to the same selective pressures, and ii) a metabolomic clock should not only capture signals of chronological age, but also reflect differences in biological age associated with the response to different selective pressures.

To test these predictions and further explore the data, we had three primary objectives:

Objective 1) To test our first predictions, we compared the metabolomes of long-standing and recently derived populations subjected to the same selection regime to evaluate levels of metabolomic convergence between them. If the known life history trade-offs that characterize the response to this selection in this system have a clear signal in the metabolome, newly derived and long-standing populations should show a high degree of metabolomic convergence within each respective regime.

Objective 2) To test our second prediction, we created separate metabolomic clocks using data from A or C-type regimes. As with previous studies, we expect that these models will capture signals associated with age. In other studies, the deviation of the clock's prediction from the chronological age of the sampled flies reflected mortality risk within the studied population. In this

159 setting however, we use such age acceleration to test our hypothesis about the relative biological
160 ages of flies from these two regimes. We expect that, relative to the metabolome of the C-type
161 populations, the A-type population metabolome will appear 'older'. Similarly, we predict that a
162 clock model based on the metabolome of the A-type populations will predict younger biological
163 age for the metabolome of the C-type populations.

164 Objective 3) To generate insights into the metabolic mechanisms underlying the
165 accelerated aging phenotype observed in flies from the A-type regime, we characterized the
166 metabolomic trajectories associated with aging in the populations under the A and C-type
167 selection regimes. We identify sets of metabolites with similar abundancies among young A-type
168 flies, and the oldest of the C type flies. We find that these sets of metabolites include many with
169 known associations with age or aging across taxa.

170

171

172 **Results**

173 *Metabolomic profiling*

174 Targeted metabolomic profiling included a panel of 361 target metabolites, 210 of which
175 were detected during LC-MS profiling, with 202 including values for all samples (see Table S1
176 for full details). Metabolite abundance values were normalized (Methods) for further analyses
177 (Table S2).

178 ***Objective 1: Metabolomic Convergence Within Selection Regime***

179 Because of the intimate connection between metabolome and physiology, we hypothesize
180 that the among-regime convergence in mortality among the more-recently derived and the long-
181 standing selection lines is paralleled by convergence in their metabolome. We tested
182 convergence among the metabolome of more-recently derived and the long-standing populations
183 in two ways, both of which test for *divergence* of the metabolome. In this way, we are asking if the
184 metabolome of recent and long-standing populations subject to the same selection regime differ
185 significantly. Such effects would be contrary to our hypothesis. First, by testing for effects of
186 selection history (recent v. long-standing) within each regime on the multivariate metabolome, and
187 second, by testing the accuracy of predictive models trained on the metabolome of long-standing

188 populations to predict the regime of more recently derived populations based on their
189 metabolome.

190 We used principal components analysis to reduce the dimensionality of the metabolome.
191 The first 12 principal components (PCs) each explain more variation than expected from
192 randomized data (Tracy-Widom test, alpha=5%). Among the first 12 metabolome PCs on the 21-
193 , 28- and 35-day timepoints, on which samples from both regimes A and C were sampled, age
194 had significant effects on the variance of PCs 3, 4 and 8, and regime had significant main effects
195 on PCs 1, 2, and 4 (ANOVA P<5% after Bonferroni correction, Methods, Figure 3). We tested for
196 divergence as interaction effects of history within regimes. We found no evidence of regime x
197 history interaction on any of the first 12 PCs, either as main effects on the PC (PC ~ regime x
198 history), or on the trajectory of PCs over age (PC ~ regime x history x age; P>5%, Figure 3,
199 Methods).

200 We then tested the accuracy of a supervised multivariate predictive model trained on only
201 the metabolome data of the long-standing populations collected on days 21, 28 and 35 (Methods).
202 This model had an accuracy in predicting the regime of >95% on the training data from long-
203 standing populations (Figure 4A), whereas on the held-out data from more recently derived
204 populations, the model predicted regime perfectly (Figure 4B). Failing to distinguish the
205 metabolome of recent and long-standing populations along any of the PCs and the high accuracy
206 of discrimination models on the recently derived metabolome suggest that the metabolome has
207 converged by regime among the recently derived populations.

208

209 ***Objective 2: Metabolomic Clocks and the Effect of Selection Regime***

210 Consistent with other phenotypes, we hypothesize that the metabolome will also serve as
211 a predictive phenotype for both chronological and biological age. We expect that, if there is a
212 detectable selection driven alteration to the metabolome, then the A-type populations will appear
213 older relative to the C-type populations of the same chronological age. To test for the signal of
214 aging in the metabolome, we constructed metabolomic “clocks” trained on metabolite abundance
215 patterns specific to each selection regime, then used those clocks to predict the age of samples
216 both within, and between regimes (Methods).

217 *Metabolomic Clock Results*

We first evaluated the relationship between the metabolome and age, separately, within the A-type and the C-type populations using within-regime elastic net regression models (clocks, Methods). The within-regime clocks of the C-type and A-type both accurately predicted the age of flies in their respective regimes, with an R^2 of 0.915 and 0.849 respectively (Figure 5). To test hypotheses about the differences in biological age, or the pace of aging in response to selection, we turned to between-regime metabolomic clocks (Methods). We fit a linear model to test for the relationship between chronological age and predicted age made by the between-regime C-type clock, when applied to the metabolome of the A-type, and compared these predictions to those of the withing-regime C-type clock (Methods, Figure 5A). The C-type clock was able to account for 91% of the aging for within-regime predictions ($\beta_0 = 0.914$), and 86% of the aging for between-regime predictions ($\beta_1 = 0.859$), accounting for a difference in predictive power that was not significant ($\beta_{dif} = -0.055$, $p > 0.6$). While the slope of the aging trajectory did not differ between the within-regime and between-regime predictions, there was a significant increase in the intercept for the A-type population age predictions of ~23 days ($\alpha_{dif} = 23.45$, $p < 1.1\text{x}10^{-9}$). Together these results suggest that, as estimated by the C-type clock, the A-type metabolome shows a consistently greater predicted age (biological age), but do not show a difference in the perceived rate of aging, when compared to the actual age (chronological age) and aging patterns of the A-type populations.

We then used the between-regime A-type clock to predict age in C-type flies and used the same linear model framework to test for effects of selection regime on age and aging in the metabolome (Figure 5B). The A-type clock accounted for 83% of the aging for within-regime predictions ($\beta_0 = 0.830$), but only 33% of the aging for between-regime predictions ($\beta_1 = 0.330$), a difference in predictive power that was significant ($\beta_{dif} = -0.50$ $p < 5.9\text{x}10^{-12}$). This difference in aging trajectories suggests a different perceived rate of aging, with the A-type clock “seeing” the C-type populations as aging more slowly relative to the A-type populations. Similar to the C-type clock results, the A-type clock also showed a significant difference in intercept ($\alpha_{dif} = 8.12$, $p < 2.8\text{x}10^{-5}$), though direct interpretation of this value is complicated as this difference is not consistent across age classes. For the timepoints where C-type samples are present, we see that the C-type population ages are predicted to be younger than their actual chronological age, showing that the A-type populations do “see” the C-type populations as younger when there are representative samples.

The A-type and C-type clocks make different age predictions on metabolome data from the two regimes sampled at the same chronological age. And yet, regardless of regime, the two

clocks predict increasing biological age as chronological age increases. We considered two possibilities, one, that the two clocks are primarily utilizing variation in the same subset of metabolites within either regime to make age predictions. Alternatively, the A- and C-type clocks could gain predictive power from two different sets of metabolites as they vary with age within-regime. To distinguish these two possibilities, we examined the coefficients fit to each metabolite within both clocks.

Both clocks used an elastic net penalty L1>0, and so at least some metabolites were given no importance. This left 27 metabolites selected as model features for the A-type clock, and 23 metabolites as model features for the C-type clock (Table S3). Of these features, five metabolites were common to both clocks (Figure 6A). An intersection of five metabolites does not indicate enrichment of metabolites among the two clocks (Fisher's test, odds ratio=1.97, P=0.20). However, the coefficients for the five metabolites common to both clocks were highly correlated (Pearson's ρ=0.96, P=0.0092, Figure 6B). In comparison to the importance (β) of the metabolites specific to the C-type or A-type clocks, the five common metabolites were not significantly more or less important within either clock (Wilcoxon's test W≥54, P≥0.54, Figure 6C).

Objective 3: Metabolomic Trajectories of Rapid Aging

To characterize the metabolomic trajectories associated with aging in the populations under the A and C-type selection regimes, we used a multifaceted approach to reveal age and regime specific patterns of metabolite abundance.

Principal components analysis revealed clustering by both selection regime and age (Figure 7A). The common ages sampled for both the A-type and C-type populations (21, 28, and 35 days) showed separation along both the PC1 and PC2 axes. The 9-day-old samples from A-type populations clustered separately from all other samples along both PC axes, showing a greater degree of differentiation for these samples than the rest. The 70-day-old samples from C-type populations were the only samples that clustered more closely with the opposing selection type, showing overlap with samples from the A-type populations at ages 28- and 35-days-old. Samples from the common ages (21, 28, and 35 days) clustered within selection regime, with some separation by age within their respective selection regimes. These patterns were consistent when selection history (recently derived or long-standing) was factored (Figure S1).

Next, a Linear Mixed-effects Model (LMM) approach was used to characterize specific patterns of metabolite differentiation (Table S4). Of the 202 metabolites in our data set, a total of 176 unique metabolites were identified as significant for at least 1 term (FDR <0.01) (Figure 7B). The selection term explained most of the difference in the metabolome, accounting for 118 of the 176 significant metabolites, 20 of which were unique to the term. The age term accounted for 107 significant metabolites, with 16 unique to the term. The interaction term accounted for 100 of the significant metabolites, with 23 unique to the term.

Characterizing Metabolite Abundance Patterns

We generated a heatmap that included mean values for each age and selection regime for the 176 unique metabolites that were significant for at least one term from the LMM (Table S4). Hierarchical clustering based on columns (representing selection regime and age in days) resulted in clusters that are consistent with the earlier PCA (Figure 7A), where A-type age 9 samples clustered independently, the matched ages (21, 28, and 35 days) clustered within regime but not across regimes, and the C-type age 70 samples clustered more closely with the matched age samples from the A-type regime than the rest of the C-type samples (Figure S2). Hierarchical clustering based on rows (mean metabolite abundance) revealed two clusters that clearly exhibited a pattern where A-type samples (aged 21, 28, 35 days) and the oldest C-type samples (aged 70 days) have metabolite abundance patterns more similar to each other than to the younger C-type samples. This pattern is consistent with the general accelerated aging phenotype observed in the A-type populations, potentially indicating an aged phenotype represented in the metabolome. To highlight this pattern, we used the subset of metabolites included in these two clusters to generate a reduced heatmap, where column clustering was maintained from the full heatmap, and rows were allowed to cluster based on the subset data, both resulting in dendrograms consistent with the larger heatmap (Figure 8). These two clusters represented either metabolites with higher abundance in the samples with an aged phenotype (cluster A), or lower abundance in samples with an aged phenotype (cluster B) relative to the younger C-type samples. These clusters contained a total of 25 metabolites, with clusters A and B containing 13 and 12 metabolites respectively (See Table 1 for details).

Discussion

Objective 1: Metabolomic Convergence Within Selection Regime

Adaptation in response to selection on reproductive timing in this system is associated with a number of physiological and developmental tradeoffs with complex genetic underpinnings. Because the metabolome constitutes the functional building blocks, and energetic currency of cells, we hypothesize that the physiological tradeoffs associated with the accelerated aging phenotype of A-type flies would be reflected in the abundancies of metabolites. Alternatively, the metabolome could associate with a wide variety of traits, only some of which are involved in the accelerated development or reduced longevity that evolve under these regimes. If our hypothesis is true, then we expect that populations under the same selection regime would show evidence of convergence within the metabolome, even in more recently selected populations. To test this prediction, we compared the metabolomes of populations from recently derived and long-standing histories under the same selection regime. We found that the metabolomes of recently derived and longstanding populations under the same selection regime were highly converged for both A- and C-type selection regimes. This was evident by both a consistent metabolomic divergence between selection regimes, and by the high accuracy of multivariate model predictions, regardless of the number of generations under selection. Overall, the high levels of metabolomic convergence within selection regimes shows that the metabolome is a reliable biomarker of the underlying physiological responses to selection.

Objective 2: Metabolomic Clocks and the Effect of Selection Regime

Over the lifespan of the fly, the dynamics of the metabolome have been used to connect advancing chronological age to the rise in mortality risk that defines biological aging (Zhao et al. 2022). Multivariate age prediction models (clocks), particularly epigenetic clocks, have been used to predict age across species (Meyer and Schumacher 2024; Lu et al. 2023). The use of clock models to understand the evolutionary process however is just beginning (Parrott and Bertucci 2019). Here we apply clock models of the metabolome to test our hypothesis that the rapid response to selection for early life reproduction is associated with the same underlying aging processes that are reflected in the metabolome. If true, the response to selection seen in the metabolome likely reflects shifts in physiological processes that are a part of normal aging in the ancestral population. If the rapid and repeatable shifts in allele frequency (Graves et al. 2017), and both transcriptomic (Barter et al. 2019) and phenotypic (Burke et al. 2016; Kezos et al. 2023)

convergence are an indication of selection acting on common physiological mechanisms, then the components of the metabolome most closely tied to aging physiology should respond similarly. A critical prediction of our hypothesis is that the relative biological age of flies under the A-type selection regime should appear 'older' than flies under the C-type selection regime.

To test this hypothesis, we first trained age prediction models *within* each regime, resulting in an A-type clock and C-type clock. Both clocks captured the monotonic increase in chronological age within each respective population, with accuracy R^2 exceeding >0.84 (Figure 5). In between-regime predictions, the C-type clock detected both the chronological age increase in the A-type flies, but also a strong age-independent increase in biological age of more than 23 days (Figure 5A). Consistent with our predictions, the C-type clock detected an increase in biological age associated with the A-type selection regime. The C-type clock did not predict a difference in slope between the regimes, indicating that, relative to the metabolome change in the C-type, the A-type and C-type appear to age at the same rate, despite the A-type flies appearing to be older.

The A-type clock detected a difference in biological age in C-type flies, though this change is less directly interpretable, and doesn't result in a fixed age difference. Consistent with our predictions, the differences in perceived rate of aging showed that, for the ages where C-type populations were sampled, the A-type model predicts them to be younger than their actual age.

The A-type clock achieved an accuracy of R^2=0.849 when predicting age in the A-type, while utilizing only 13.4% of 202 metabolites, and the C-type clock utilized only 11.4% to achieve even higher accuracy R^2=0.915. Independently fit to two different data, the C-type and A-type clocks utilized predominantly non-intersecting metabolites, however they both included five intersecting metabolites (Figure 6A, Table S3). While this number of intersecting metabolites is not more than expected by chance, the coefficients fit to these metabolites in both clocks were highly correlated, indicating a common axis of variation with age in the metabolome. We note that, while correlated, the coefficients fit from the A-type clock tend to be greater than those of the C-type clock (Figure 6B). This seems to reflect the relative pace of aging in these two populations. The larger coefficients fit to predict age in the more slowly aging C-type populations could result in higher predicted ages when predicting age on the A-type metabolome.

It is important to note that, while the metabolites identified by the clock models shed light on the underlying metabolome variation related to age and to aging, elastic net and other regularized regression methods are designed in part to reduce the influence of co-linear predictors (Zou and Hastie 2005; Bujak et al. 2016). Because of this, the set of metabolites most influential in clock models may not include metabolites that share very similar age-related variation in abundance, and so do not give a complete picture of age-associated metabolome variation in

which collinearity is common (Lassen et al. 2023; Avanesov et al. 2014). In this light, we turn to a descriptive analysis of the metabolome variation and its convergence within regime to describe the patterns of variation under these selection regimes.

Objective 3: Characterizing Metabolite Abundance Patterns

The metabolite abundance patterns depicted in Figure 8 are consistent with the prediction that the aging phenotype, shared by both the older C-type and younger A-type flies, would be present in the metabolome. This similarity in the metabolomes of old C-type and younger A-type flies is consistent with a broad array of age-related phenotypes shared by these two groups of flies, including high mortality rates (Figure 2), as well as reduced egg viability (Chippindale et al. 1997), stress resistance (Kezos et al. 2023), and fecundity (Burke et al. 2016).

This metabolomic similarity suggests that these clusters (A and B) contain metabolites associated with the accelerated aging phenotype of A-type flies. In fact, a literature search revealed that more than half of the metabolites included in these two clusters have previously been associated with aging (Table 1). For example, cluster A contains L-Kynurenine, a tryptophan metabolite, that has been associated with aging in mice (Elmansi et al. 2020), and Allantoin, an end product in purine metabolism, that has been associated with aging in flies, especially in populations that age more rapidly (Yamauchi et al 2020). In the cases of both L-Kynurenine in mice, and Allantoin in flies, these metabolites were elevated in animals at advanced ages, which is consistent with metabolite abundance patterns for the accelerated age phenotype flies found in cluster A. Similarly, cluster B contains Carnitine and Succinyl-carnitine, both of which are involved in lipid metabolism and energy production and are associated with aging in rats (Garvey et al 2014). Both Carnitine and Succinyl-carnitine were decreased in rats at advanced ages, which is consistent with the metabolite abundance patterns for the accelerated age phenotype flies found in cluster B.

The correspondence of these known age-associated metabolites with selection-related abundance patterns suggests that these clusters (A and B) contain good candidates for future research on aging and longevity. Additionally, metabolites found in those same clusters are also implicated in metabolic disfunction, such as insulin resistance and lipid metabolism disorders across taxa (Table 1). With nearly half of the metabolites in cluster A implicated in metabolic disfunction, alterations to metabolic processes likely play a role in the accelerated aging phenotype exhibited by flies under the A-type selection regime.

405 **Conclusion**

406 We set out to investigate the metabolomic signal of accelerated aging associated with
407 selection for early reproduction. We found a high degree of metabolomic convergence between
408 recently derived and long-standing populations of *D. melanogaster* under the same selection
409 regime, consistent with other phenotypic convergence previously described in this system. As
410 such, the evolutionary repeatability that defines adaptation in this system also extends to the
411 metabolome. Using the metabolome as a predictor of age revealed both a general metabolomic
412 signal of aging, and a metabolomic signal of selection regime differences in biological age.
413 Characterizations of metabolomic change associated with selection regime indicate new
414 candidates for metabolites that play a role in the accelerated aging phenotype. This work
415 demonstrates the viability of metabolomic phenotyping as a tool for those seeking to use
416 experimental evolution to identify factors underlying complex trait variation.

Materials and Methods

Experimental Populations

All 20 *D. melanogaster* populations used in this study share a common origin, traced back to the large and outbred Ives (1970) population. Numerous populations have been derived from this wild-bred lineage, first by Michael Rose and Brian Charlesworth (Charlesworth 1980; Rose & Charlesworth 1980; Rose & Charlesworth 1981; Rose 1984) and then by generations of the Rose Lab (e.g. Chippindale 1997, Burke et al. 2016), to study the evolutionary theory of aging. All populations in this system are maintained at census sizes of ~2000 individuals in an attempt to keep them outbred. Based on past genomic studies, we know there is abundant genetic variation in all populations even after many hundreds of generations of evolution (e.g. Phillips et al. 2016; Graves et al. 2017). Here we focused on the A-type populations and their controls, the C-type populations (Figure 1B). A-type populations were maintained on a 10-day generation cycle, whereas the C-type populations were maintained on a 28-day cycle. As a result of this difference, the A-type populations exhibit accelerated development, reduced longevity, higher early-life fecundity, and lower stress tolerances than to the C-type populations (Burke et al. 2016; Kezos et al. 2023). There are two selection histories within the A and C-type populations, ACO/AO and CO/nCO, respectively (See Figure 1A). Each history is distinguished by the number of generations they have been under selection, with AO and nCO having been derived more recently than ACO and CO to test questions about evolutionary repeatability (see Burke et al. 2016 and Graves et al. 2017). We know that populations from these selection histories that share the same selection regime have converged at several phenotypic levels and recent studies have treated them as replicates within each regime (A or C), based on phenotypic (Burke et al. 2016), genomic (Graves et al. 2017), and transcriptomic (Barter et al. 2019) studies. At the time of sampling for this project, the ACO and AO populations had ~1,000 and ~490 generations under selection, respectively, whereas the CO and nCO populations had ~415 and ~160 generations, respectively. In all of the experiments described here, we include five historical replicate populations of each of the four experimental populations (ACO, AO, CO and nCO), that have been maintained as independent lineages for the entirety of the generations under each selection regime.

Mortality Assays

Adult mortality assays were based on published protocols (Burke et al., 2016) which measured mortality in the same five replicate populations of each of the four experimental populations ACO, AO, CO, and nCO. Prior to measurement, all of the experimental populations

were maintained on a 14-day culture cycle for two generations, staggered a day apart, to align the different treatments to a shared calendar and reduce the impact of gene by environment interaction. Each replicate was expanded into two cohorts (e.g. ACO1α & ACO1β) of ~1,500 flies, each in a Plexiglas cage, supplied with fresh banana-molasses based media (as described in Phillips et al. 2018) each day with yeast solution to induce oviposition once transferred on day 14 from egg. Ambient temperature was maintained at ~25 ˚C throughout. At the same time each day, all dead flies were removed from each cage to be sexed and logged until no living flies remained. Mortality data was pooled between the two cohorts for each population to give the total number of deaths per day of each population. Age specific mortality (*M*) was calculated as follows:

$$M = \frac{n_d - n_{d-1}}{n_{d-1}}$$

Where *n* equals the number of flies alive on a given day (*d*), and *d* -1 represents the day prior. The Burke et al. (2016) protocol was modified for this experiment to remove the use of carbon dioxide in condensing cohorts when census densities were sufficiently low. Instead, flies within cohorts remained in the same cage for the duration of the experiment, regardless of census density, and the inside of the cages were cleaned as needed to remove waste build-up.

Sample Collection

Samples were collected for metabolomics using protocols described by Phillips et al. (2022). A cage-cohort of ~1,500 flies was generated from each of the five replicate populations for ACO, AO, CO, and nCO and maintained on a 14-day culture cycle for two generations, staggered a day apart to mitigate the impact of gene-by-environment interactions. Cohorts were maintained in a Plexiglas cage and were fed fresh banana-molasses based media each day with yeast solution to induce oviposition. Concurrent to the mortality experiment, the five replicate cage-cohorts for each selection history were sampled for metabolomic extraction at multiple timepoints (9 days for A-type populations, 21, 28, and 35 days for all populations, and 70 days for C-type populations). Metabolomic profiles are highly sexually dimorphic within the *Drosophila* system (Hoffman et al. 2014). In order to facilitate the large sample sizes and sampling time points needed, as well as to reduce the potential noise caused by using both sexes within pooled samples, we focused on females in our sampling effort. Each sample consisted of a pool of ~50 female flies that were randomly drawn from each population per timepoint. An equivalent number of males were removed from populations for each sample to maintain population sex ratios. While

480 metabolomic characterization can be done with far fewer than 50 flies, the populations featured
481 in this study are outbred and still harbor a great deal of genetic variation (see Graves et al. 2017).
482 Using pool sizes of ~50 flies was an attempt to capture and represent this variation. The pooled
483 samples were immediately dry frozen in liquid nitrogen and stored at −80°C prior to metabolite
484 extraction. Due to decreased population sizes at late ages, two samples contained less than 50
485 flies: ACO_1 day 35 (n= 25), and nCO_4 day 70 (n= 36). These populations were selected based on
486 their generation cycle rather than the number of days since eclosion, so age is consistently
487 referred to as the time since egg deposition throughout the manuscript.
488 The time points used in this study were informed by demographic data and prior studies
489 of flies under these regimes. Burke et al. (2016), and Barter et. al (2019) characterized mortality
490 rates within the A-type and C-type regimes and they defined the "aging" or "non-aging" phases of
491 their lifespan. For the A-type regime, day 9 from oviposition represents a uniquely non-aging
492 phase of the accelerated lines whereas day 21 shows the onset of a rapid aging phase (Figure
493 2). Conversely, the C-type regimes were sampled in parallel on days 21, 28, and 35, but were
494 only expected to exhibit the aging phase starting at day 35 (Figure 2).
495
496 *Sample Preparation*

497 Aqueous metabolites for targeted liquid chromatography–mass spectrometry (LC-MS)
498 profiling of 80 fly samples were extracted using previously described protein precipitation method
499 (Kurup et al. 2021; Meador et al. 2020). Briefly, samples were homogenized in 200 µL purified
500 deionized water at 4 ˚C, and then 800 µL of cold methanol containing 124 µM 6C13-glucose and
501 25.9 µM 2C13-glutamate was added. Internal reference standards were added to the samples to
502 monitor sample preparation. Next, samples were vortexed, incubated for 30 minutes at -20˚C,
503 sonicated in an ice bath for 10 minutes, centrifuged for 15 minutes at 14,000 rpm at 4˚C, and then
504 600 µL of supernatant was collected from each sample. Lastly, recovered supernatants were dried
505 on a SpeedVac and reconstituted in 0.5 mL of LC-matching solvent containing 17.8 µM 2C13-
506 tyrosine and 39.2 3C13-lactate, and internal reference standards were added to the reconstituting
507 solvent to monitor LC-MS performance. Samples were transferred into LC vials and placed into a
508 temperature-controlled autosampler for LC-MS analysis.
509
510 *LC-MS Assay*

511 Targeted LC-MS metabolite analysis was performed on a duplex-LC-MS system composed of
512 two Shimadzu UPLC pumps, CTC Analytics PAL HTC-xt temperature-controlled auto-sampler

513 and AB Sciex 6500+ Triple Quadrupole MS equipped with ESI ionization source (Meador et al.
514 2020). UPLC pumps were connected to the autosampler in parallel and were able to perform two
515 chromatography separations independently from each other. Each sample was injected twice on
516 two identical analytical columns (Waters XBridge BEH Amide XP) performing separations in
517 hydrophilic interaction liquid chromatography (HILIC) mode. While one column was performing
518 separation and MS data acquisition in ESI+ ionization mode, the other column was equilibrated
519 for sample injection, chromatography separation and MS data acquisition in ESI- mode. Each
520 chromatography separation was 18 minutes (total analysis time per sample was 36 minutes), and
521 MS data acquisition was performed in multiple-reaction-monitoring (MRM) mode. The LC-MS
522 system was controlled using AB Sciex Analyst 1.6.3 software. The LC-MS assay targeted 361
523 metabolites and 4 spiked internal reference standards. Measured MS peaks were integrated using
524 AB Sciex MultiQuant 3.0.3 software. Up to 210 metabolites and 4 spiked standards were
525 measured across the study set, and over 90% of measured metabolites were measured across
526 all the samples. In addition to the study samples, two sets of quality control (QC) samples were
527 used to monitor the assay performance and data reproducibility. One QC [QC(I)] was a pooled
528 human serum sample used to monitor system performance and the other QC [QC(S)] was pooled
529 study samples, were used to monitor data reproducibility. Each QC sample was injected for every
530 10 study samples. We assessed the reproducibility of the LC-MS using the coefficient of variation
531 (CV) of each of the 202 metabolites among 10 technical replicates. The mean CV was 0.0044
532 with a range of $6x10^{-4}$ to 0.029 (Figure S3). Raw results from LC-MS can be found in Table S1.
533
534 *Data Processing and Normalization*

535 The LC-MS data was filtered and normalized prior to analysis. Any metabolites with
536 missing values were removed from the data set, and relative peak areas for the remaining 202
537 metabolites were log-transformed to approximate a Gaussian distribution. Next, within sample
538 metabolite data were mean-centered to account for sample-to-sample variation. Given that the
539 LC-MS profiling was performed in three separate batches over three days, we estimated main
540 effects of batch (*B*) on each metabolite and corrected for these batch effects by taking the
541 residuals (ε) of the following linear model:

542 $$Metabolite = B + \varepsilon$$

543 These residuals then constitute the normalized abundance measures for 202 metabolites
544 across 80 fly samples (Table S2).
545

546 ***Objective 1: Metabolomic Convergence Within Selection Regime***

547 To test for divergence between recent and long-standing populations in the multivariate
548 metabolome, we first conducted a Principal Components (PC) Analysis (PCA) using the prcomp
549 R package. We then fit the fixed effects of age (as an ordered categorical factor), regime (A-type
550 or C-type), history (either recent or long-standing), their interactions, and a random effect of
551 replicate on the eigenvalues of each of the first 12 PCs (PC_x) by ordinary least squares in the
552 lme4 R package (Bates et al. 2015).

553 $$PC_x \sim \alpha + \ age \ \times \ regime \ \times \ history + 1|replicate + \ \varepsilon$$

554

555 This analysis was limited to the most directly comparable data between regimes, those
556 from day 21, 28, and 35. As a liberal test for divergence, a result that is contrary to our hypothesis,
557 we simply ask if there was either a regime x history interaction effect, *or* a regime x history x age
558 effect on *any* of the first 12 PCs at a P value of <0.05, without adjusting for the 12 tests (each of
559 PC 1 to 12).

560 To test the potential of the metabolome of long-standing populations to predict selection
561 regime in the recently derived populations, we trained a partial least-squares model to predict
562 regime with the data from the long-standing populations, by 5-fold cross-validation (CV) in the
563 caret R package. This model was then used to predict regime among the samples of the more
564 recent populations. In both training and prediction, only the data from day 21, 28, and 35 were
565 used. The accuracies of the model on the training data (long-standing), and on the held-out data
566 from the recent populations was assessed by receiver operating characteristic (ROC) curve.

567 ***Objective 2: Metabolomic Clocks and the Effect of Selection Regime***

568 *Elastic Net Regression Models and Analysis*

569 We used two approaches to generate predicted ages for the flies based on the
570 metabolome data, both of which needed a different approach to, in all cases, avoid age predictions
571 for biological replicates that were part of the model training data. The first approach, whose goal
572 was to generate *within-regime* predictions, required clocks trained and then tested on data from
573 the same regime. The second approach, whose goal was to generate regime-specific models
574 only to then predict ages for the opposite regime. These later clocks we refer to as *between-*
575 *regime*.

576 *Within-regime prediction:* For the within-regime predictions, we used an iterative leave-one-
577 replicate-out (LORO) strategy on each regime separately. At each iteration of the LORO
578 procedure, all four samples from one replicate were withheld. This was done to avoid overfitting
579 our data and producing overly generous models. See Figure S4 for an example of this
580 phenomenon where the training data has an R^2 predictive accuracy of 0.997 while the test data
581 has an R^2 predictive accuracy of 0.832. A 5-fold CV elastic net model was then trained to use the
582 metabolome data of the remaining nine replicates (n=36 samples) to predict their 36 ages using
583 the glmnet package in R (Friedman et al 2023), as discussed in Zhao et al. (2022). The predations
584 from training were not used in the final analysis, only to tune the model during 5-fold CV. During
585 the 5-fold CV, the elastic net penalty parameters L1 and L2 were selected from the default tuning
586 grid in glmnet as those that gave the lowest root mean squared error (RMSE). The model from
587 each LORO iteration was then used to predict the ages of the held-out replicate, and these
588 predictions were used in the clock analysis presented in the main text. This procedure was
589 repeated until all replicates had age predictions from a model that was trained on the data from
590 the remaining replicates within the same regime.

591 *Between-regime prediction*: For the between-regime predictions, 5-fold CV elastic net models
592 were trained on all data (n=40 samples) and ages within each regime. The between-regime
593 predictions that were analyzed in the main text were then made by the between-regime clock
594 predicting the ages of the opposite regime. So, together, the within-regime and between-regime
595 strategies resulted in predictions made on data that were not a part of model training.

596 To compare the feature importance in the between-regime A-type and C-type clocks, we
597 used the coefficients (β) fit to each metabolite in the respective clock models. For both clocks,
598 the elastic net penalty L1 at the lowest RMSE was >0, and so some metabolites have $\beta = 0$ and
599 are not features in the respective clocks.

600 We tested the accuracy of the within-regime predictions with the coefficient of
601 determination, R^2 (Kvalseth 1985; Alexander et al. 2015). Where y_i (i= 1, …, n) are the ages of
602 the test set, and $\hat{y}_i$ are the predicted ages. $\overline{y_i}$ is the mean of y_i, then R^2 is calculated as:

603 $$R^2(y, \hat{y}) = 1 - \frac{\sum_{i=1}^{n}(y_i - \hat{y}_i)^2}{\sum_{i=1}^{n}(y_i - \overline{y_i})^2}$$

604 Where an R^2 closer to 1 represents a better fitting model.

To test our hypothesis that between-regime predictions will reflect accelerated aging within the metabolome, we used a linear model to compare the predicted ages to the actual ages from the within-regime model to the between-regime model by testing differences in their slopes and intercepts using the following equations:

$$predicted\ age = \alpha_0 R_w + \beta_0 R_w + \alpha_1 R_b + \beta_1 R_b + \varepsilon$$

$$\alpha_{dif} = \alpha_1 - \alpha_0$$

$$\beta_{dif} = \beta_1 - \beta_0$$

Where α represents the intercept and β represents the slope of the regression line R_w (within-regime predictions) or R_b (between-regime predictions). With the expectation that if the accelerated aging phenotype of the A-type populations is reflected in its metabolome, then age predictions made using the C-type clock would result in a general increase in predicted biological age (α_{dif}>0) and predicted rate of biological aging (β_{dif}>0) for A-type populations. Similarly, age predictions made using the A-type clock would result in a general decrease in predicted biological age (α_{dif}<0) and predicted rate of biological aging (β_{dif}<0) for C-type populations.

Objective 3: Metabolomic Trajectories of Rapid Aging

Principal Components Analysis

To determine the extent to which metabolomic profiles cluster by age and selection treatment, a principal components analysis (PCA) was conducted on a covariance matrix of the normalized abundance data using the stats package (version 4.3.1) in R, and data visualization was conducted using the ggplot2 package (3.4.4) in R (Wickham, 2016).

Metabolomic Differentiation Between Selection Regimes

A LMM was used to compare the metabolite levels between populations under different selection regimes, either A-type or C-type, over time to test for the effects of selection, age, and the interaction between selection and age on the normalized abundance data:

$$Metabolite = \mu + Sel + Age + (Sel \times Age) + Rep + \varepsilon$$

Where selection regime (*Sel*) and age from egg (*Age*) were treated as fixed effects and replicate population (*Rep*) a random effect. We corrected for false discovery using Benjamini Hochberg (1995) approach with a corrected significance threshold of FDR < 0.01. This model was compared to a larger model that accounted for differences between the long-standing populations, and the more recently derived populations (e.g. ACO, AO, etc.), using the Akaike information criterion (AIC). However, adding this term did not improve the fit of the model (see Table S6 for results). The results of the LMM were visualized as an UpSet plot made using the UpSetR package (1.4.0) in R (Conway et al. 2017). The UpSet plot depicts the number of metabolites that were significant for each of the regression terms (FDR < 0.01), as well as the number of significant metabolites shared between any combination of the terms.

Characterizing Metabolite Abundance Patterns

To characterize metabolite abundance patterns associated with the accelerated aging phenotype observed from the A-type selection regime, we compared normalized metabolite abundance patterns for different age classes between selection regimes. First, we narrowed the metabolites of interest by filtering out any that were not significant for at least one term from the LMM results (FDR<0.01), then we calculated mean normalized abundance of each metabolite at each age within each selection regime (Table S5). We then used the pheatmap package in R (Kolde 2022) to generate a heatmap with hierarchical clustering based on the Euclidean distance and complete linkage to organize both rows (metabolites) and columns (selection regime and age) by similarity in the patterns of metabolite abundance.

655 **Data Availability**

656 Raw metabolomic and mortality data are available through Dryad
657 (https://doi.org/10.5061/dryad.1ns1rn92x) and scripts used to process and analyze data are
658 available through Github (https://github.com/mphillips67/A-and-C-Metabolomic-Trajectory-
659 Project).

660

661 **Figures**

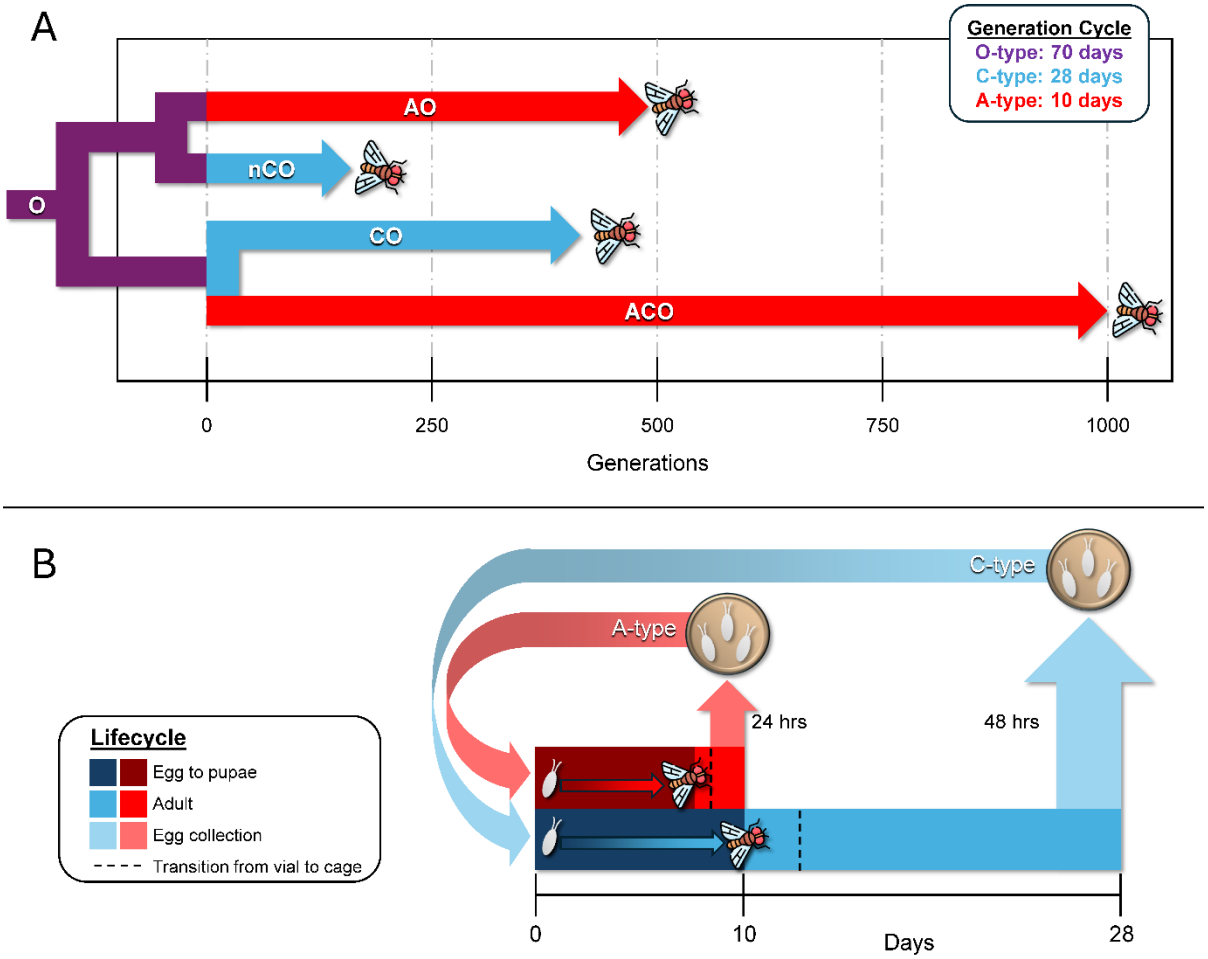

662

663 **Figure 1. Recent phylogeny and selection regimes for *D. melanogaster* populations of**
664 **interest.** A: Abbreviated diagram of the evolutionary relationship between the populations of
665 interest. The ancestral population for all populations was maintained on a 70-day generation cycle
666 (O-types), both the long-standing (CO) and recently derived (nCO) C-type populations have been
667 maintained on 28-day generation cycles, and both the long-standing (ACO) and recently derived
668 (AO) A-type populations have been maintained on 10-day generation cycles. B: Experimentally
669 controlled reproductive windows used to maintain the two life-history regimes: Accelerated (A),
670 with a 10-day reproductive cycle; and Delayed (C), with a 28-day reproductive cycle. Short
671 reproductive windows, either 24 hours for Accelerated or 48 hours for Delayed, were used to
672 enforce reproductive cycle length.

673

674

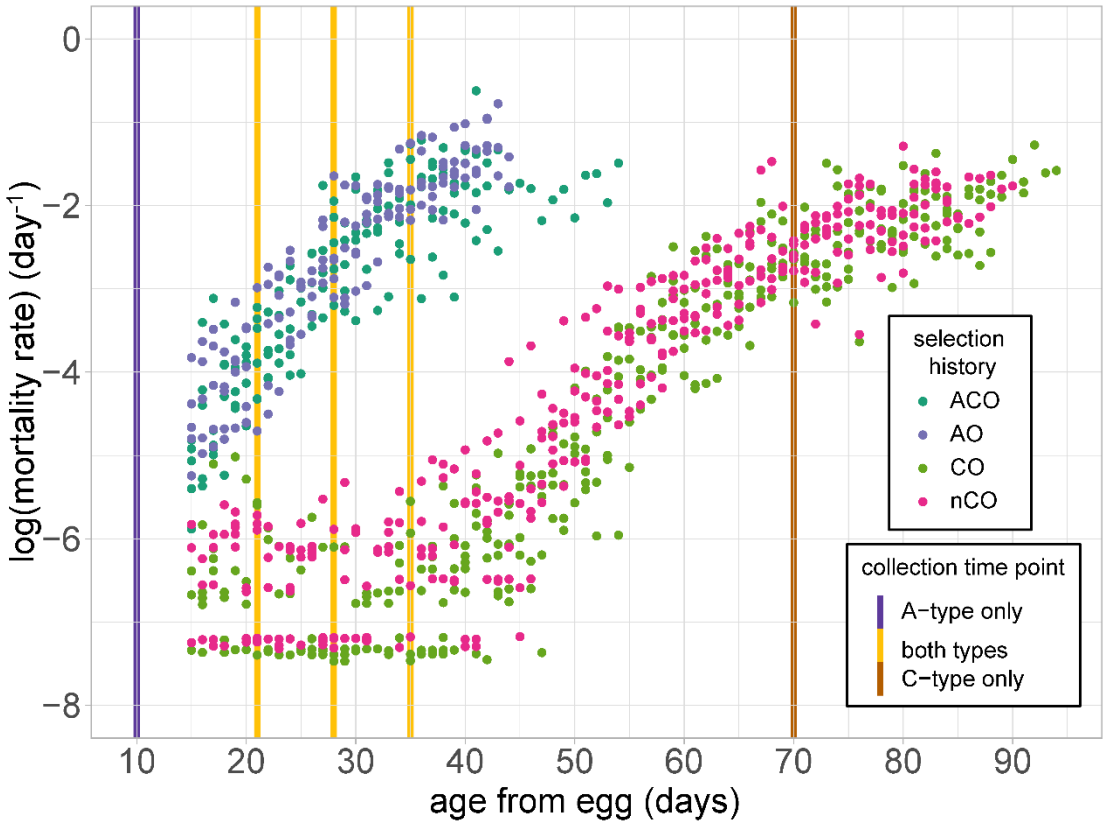

Figure 2. Age-specific mortality and metabolomic sampling design. Female mortality rates for 20 cohorts of A-type (blue and purple) and C-type (pink and green) populations (See methods for calculation). Selection history is further indicated by color, with ACO and CO representing long-standing populations and AO and nCO representing recently derived populations. Each vertical bar represents the collection timepoint in either A-type (blue), C-type (orange) populations, or both (yellow).

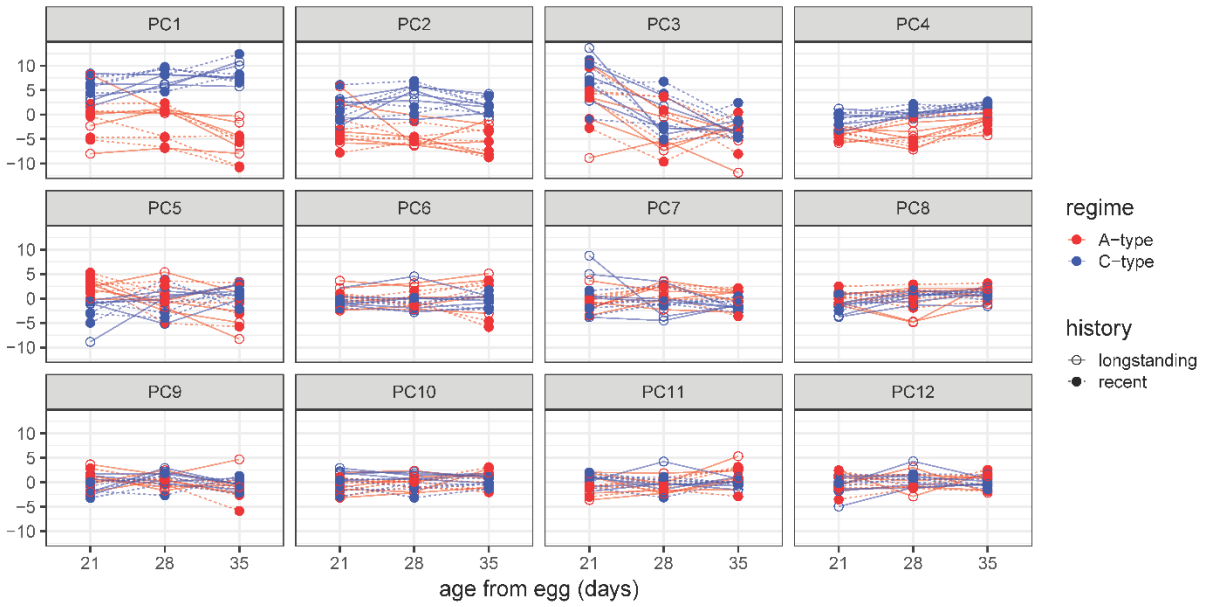

Figure 3. The metabolome and its age-trajectory converge under each selection regime. Each of the first 12 principal components of the metabolome are plotted over age, from egg (days), for the five biological replicates of each selection regime (A-type or C-type) and selection history (long-standing or recently derived). Ages in which both regimes are sampled are shown for direct comparison. ANOVA indicated that PCs 1, 2 and 4 were associate with regime, and PCs 3, 4, and 8 associate with age ($P<0.05$, after Bonferroni correction). No PCs had a significant history x regime interaction which would be inconsistent with convergence of the metabolome by regime in the long-standing and more recently derived populations.

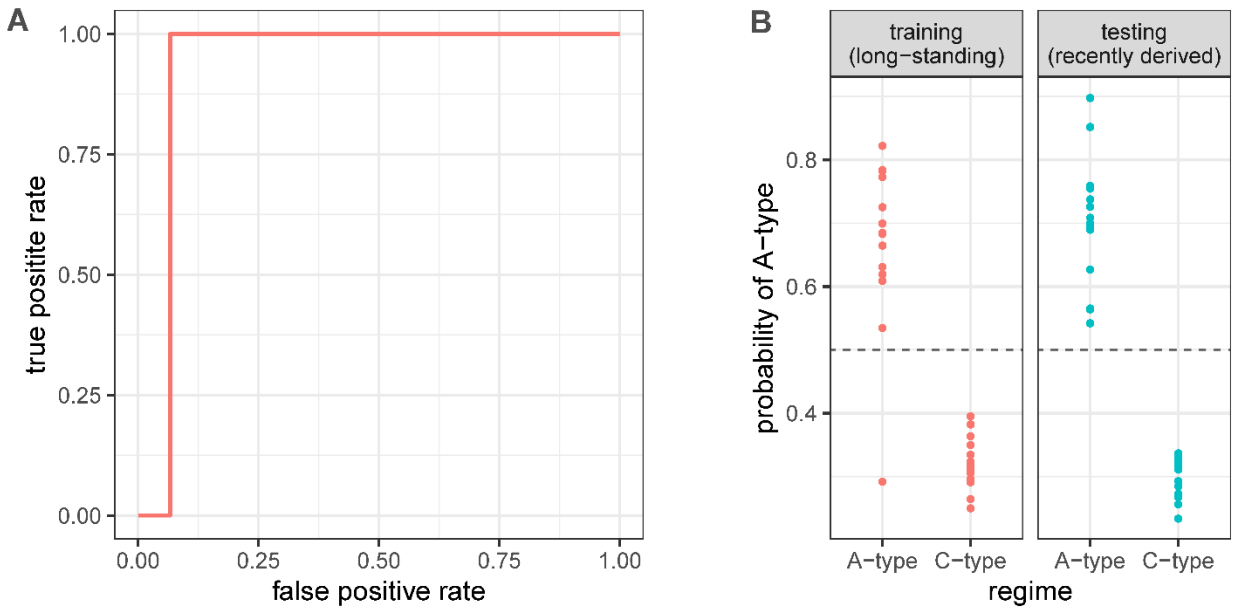

Figure 4. Regime is accurately predicted from the metabolome of the recently derived selection lines. A 2-component partial least-squares discrimination model was trained, by 5-fold cross-validation, to distinguish regime (A-type or C-type) among the 30 samples of the long-standing populations using the data from 202 metabolites. A) the 'ROC' curve for the training data. Accuracy in the training data was 96.7% in the final model, with an area under the ROC curve of 0.975. B) The probability of A-type for each of the 30 samples from the model training set (training, long-standing, and the 30 withheld samples from the recently derived populations). Discrimination is made at the 0.5 probability (dashed line). The model distinguished all samples in the test set with 100% accuracy.

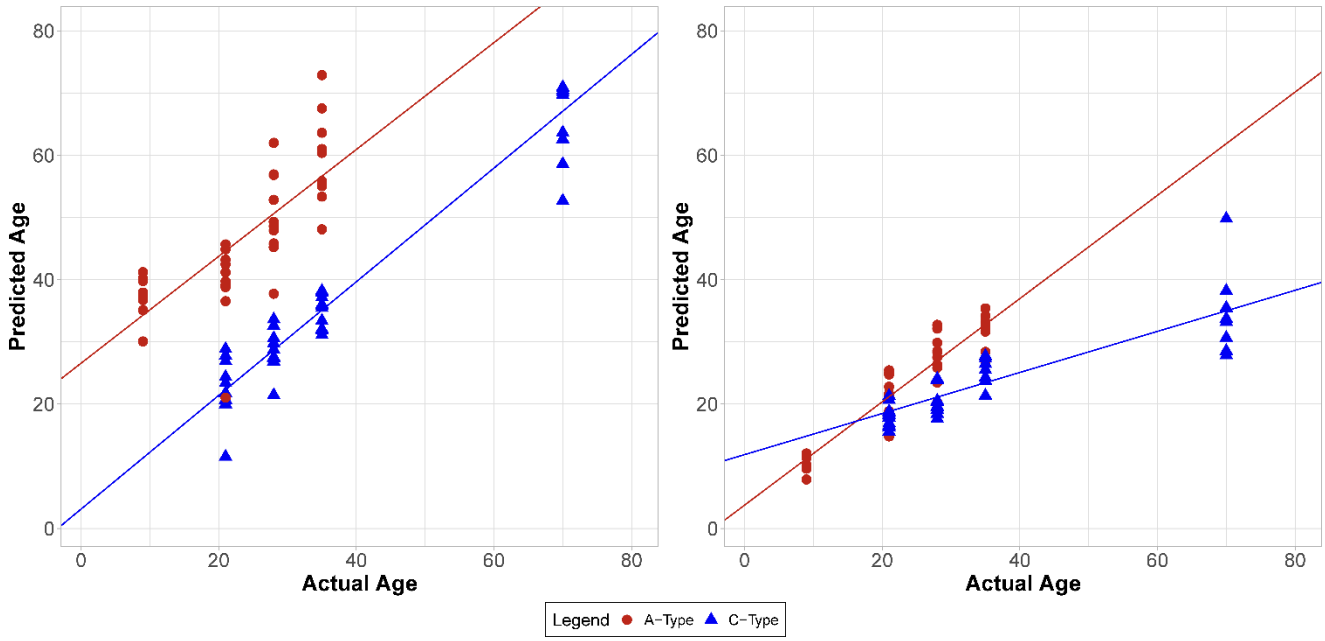

Figure 5. Selection led to different aging trajectories in the metabolome. Predicted age from egg (days) vs chronological age from egg (days) for A-type (red) and C-type (blue) populations based on elastic net models trained on metabolite data from C-type populations (A) or A-type populations (B). Points are predictions from samples held out during training (Methods). The within-regime accuracies of each model were (C-type R^2= 0.915; A-type R^2= 0.849). Lines are the least-squares fits of a linear model (Methods).

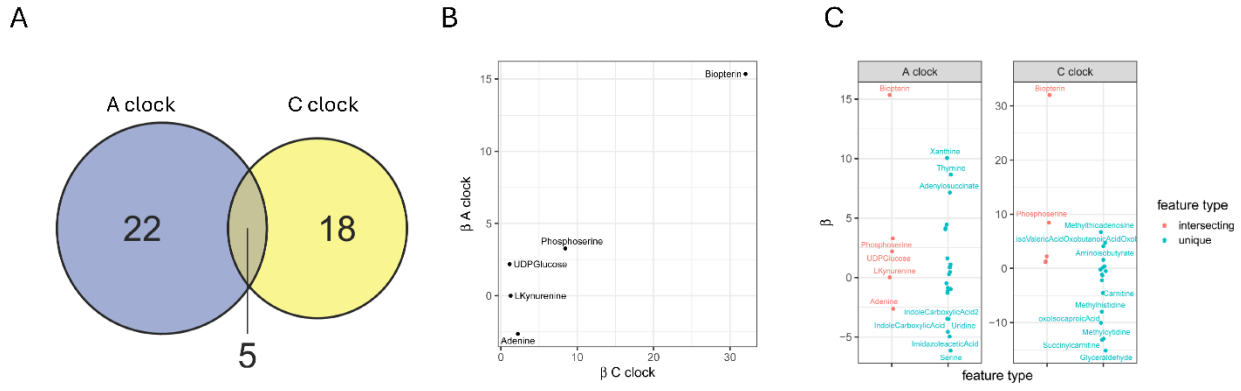

Figure 6. Metabolomic clock features. A: A Venn diagram showing the intersection among the 27 metabolites selected (β>0) by the A-type clock (blue), the 23 selected by the C-type clock (blue), with 5 selected by both clocks. B: The coefficients (β) fit to each of the 5 metabolites common to the A- and C-type clocks (Pearson's ρ=0.96, P=0.0092). C: Comparing the distribution of β fit to metabolites common to both clocks (intersecting) and the metabolites unique to each clock. There was not a significant difference in the $|\beta|$ for intersecting and unique metabolites in either clock (Wilcoxon rank sum test, W≤54, P>0.54).

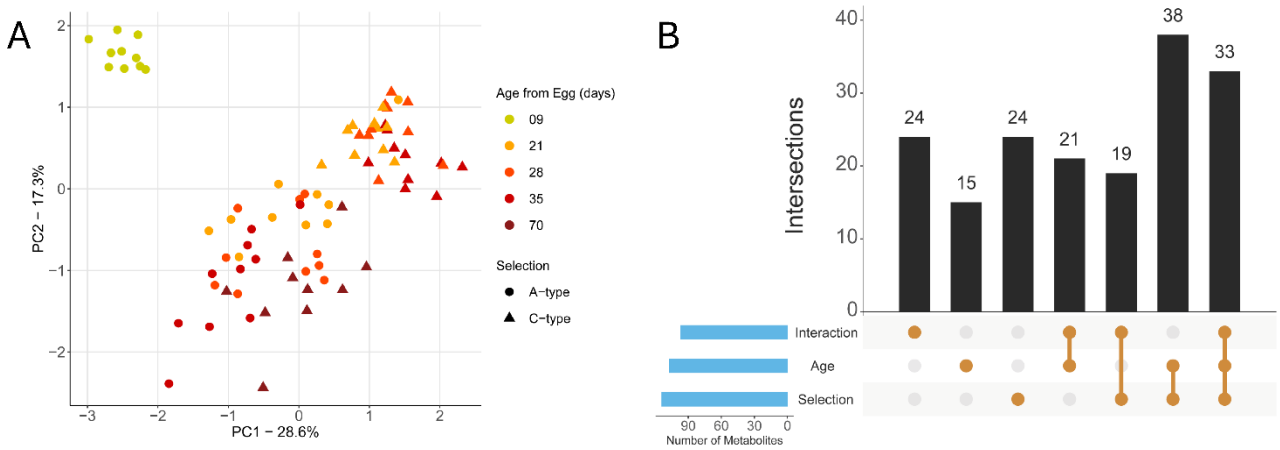

Figure 7. **Differences in metabolite abundance between selection regimes over time.** A: Principal component analysis (PCA) plot shows how samples cluster by Age (from egg, days) and Selection regime based on relative metabolite abundance along the first principal component (PC1) and the second (PC2). The percentage of variance in the metabolome explained by each PC is shown. B: UpSet plot depicting the number of metabolites that were significant from LMM (FDR <0.01) by each term: Selection, age, and the interaction along the lower left, and the number of metabolites that are significant for each term individually and each combination of terms (Intersections) along the top.

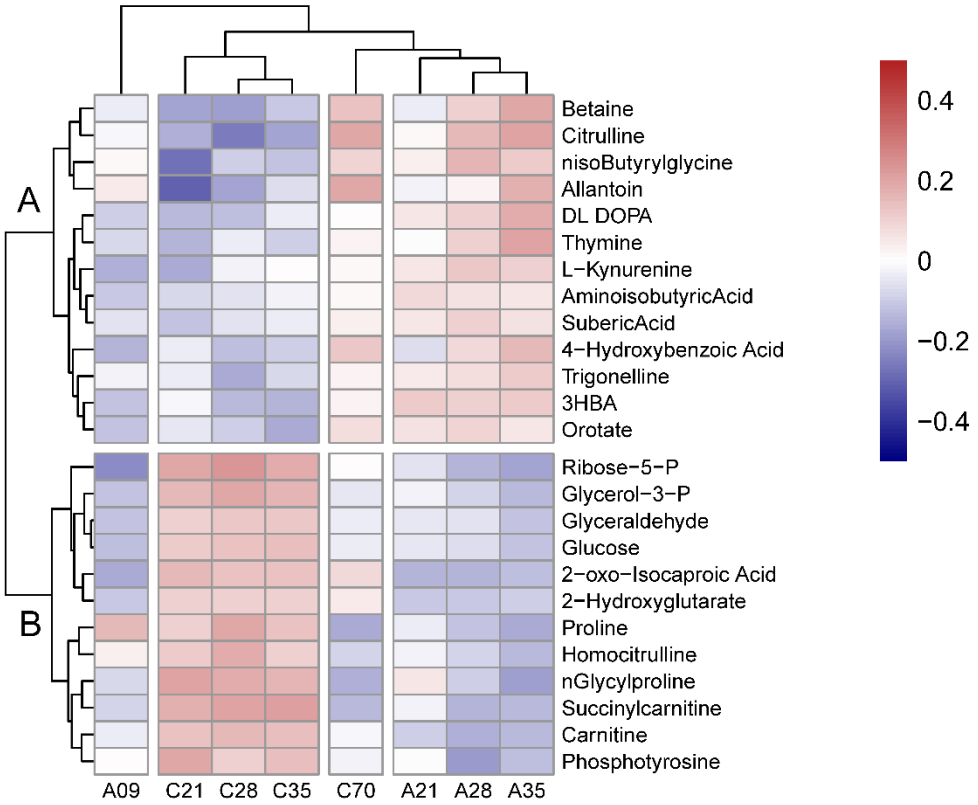

Figure 8. Hierarchal clustering of mean normalized metabolite abundance clustered by regime and age. The dendrograms were generated using 176 metabolites that were significant for any term from LMM (Table S5). See Figure S2 for heatmap that includes all 176 metabolites. Clusters (A and B) show examples where C-type age 70 days have metabolite abundance that more closely resembles the A-types than the C-types at younger ages.

Tables

Table 1. Metabolites found in clusters A and B from Figure 8 and the literature implicating them in aging or metabolic disfunction.

Cluster	Metabolite	Aging	Metabolic disfunction
A	Betaine	22	
	Citrulline	1	
	n-isoButyrylglycine		
	Allantoin	18	
	DLDOPA		
	Thymine		
	L-Kynurenine	3	10
	2-Aminoisobutyric Acid		14
	Suberic Acid	13	8
	4-Hydroxybenzoic Acid	9	
	Trigonelline	20	11
	3-Hydroxybutyric acid	5	17
	Orotate		6
B	Ribose-5-P		
	Glycerol-3-P	7	
	Glyceraldehyde		
	Glucose	12	
	2-oxo-Isocaproic Acid		
	2-Hydroxyglutarate	16	
	Proline	21, 12	
	Homocitrulline		19
	n-Glycylproline		
	Succinylcarnitine	4	
	Carnitine	4, 12, 15, 16	
	Phosphotyrosine		2

[1]Chaleckis et al 2016; [2]Dittmann et al 2019; [3]Elmansi et al 2020; [4]Garvey et al 2014; [5]Ge et al 2021; [6]Han et al 2016; [7]Houtkooper et al 2011; [8]Inouye et al 2000; [9]Kim et al 2014; [10]Kozieł et al 2023; [11]Liang et al 2023; [12]Maslov et al 2021; [13]Navas-Enamorado et al 2024; [14]Palomino-Schätzlein et al 2018; [15]Son et al 2012; [16]Wang et al 2018; 17Xiang et al 2021; [18]Yamauchi et al 2020; [19]Yang et al 2021; [20]Zeng et al 2021; [21]Zhao et al 2022; [22]Zhuang et al 2021

Acknowledgments

This work was supported by the Instrumentation Grant of the National Institutes of Health (NIH S10 OD021562), and by the Nathan Shock Center for Excellence in Basic Biology of Aging (NIH P30 AG013280). The UNCF/Bristol-Myers Squibb E.E. Just Faculty Fund, Career Award at the Scientific Interface (CASI Award) from Burroughs Welcome Fund (BWF) ID # 1021868.01, BWF Ad-hoc Award, NIH Small Research Pilot Subaward to 5R25HL106365-12 from the National Institutes of Health PRIDE Program, DK020593, Vanderbilt Diabetes and Research Training Center for DRTC Alzheimer's Disease Pilot & Feasibility Program. CZI Science Diversity Leadership grant number 2022- 253529 from the Chan Zuckerberg Initiative DAF, an advised fund of Silicon Valley Community Foundation to A.H.J. The Howard Hughes Medical Institute Hanna H. Gray Fellows Program Faculty Phase (Grant# GT15655 awarded to MRM) and the Burroughs Welcome Fund PDEP Transition to Faculty (Grant# 1022604 awarded to MRM). We thank Dr. Michael Rose at UC Irvine for sharing his experimentally evolved fruit fly populations.

Author Contributions

M.A.P. conceptualized and oversaw the project. M.A.P., K.R.A., and Z.G.G. designed the experiment. A.P., R.D.R, and V.V.C. collected all fly samples for metabolomics and carried out mortality assays under the supervision of K.R.A. D.D. and D.R. processed samples for metabolomic characterizations. T.B.B. analyzed mortality data. D.L.H, Z.G.G., and B.R.H. analyzed the metabolomic data. D.L.H., A.H. Jr., Z.V., and M.R.M developed possible functional interpretation of metabolomic results. D.L.H., M.A.P, and B.R.H. wrote the manuscript.

References

Alexander, D. L. J., Tropsha, A., & Winkler, D. A. (2015). Beware of R2: Simple, Unambiguous Assessment of the Prediction Accuracy of QSAR and QSPR Models. *Journal of Chemical Information and Modeling*, *55*(7). https://doi.org/10.1021/acs.jcim.5b00206

Avanesov, A. S., Ma, S., Pierce, K. A., Yim, S. H., Lee, B. C., Clish, C. B., & Gladyshev, V. N. (2014). Age- and diet-associated metabolome remodeling characterizes the aging process driven by damage accumulation. *ELife*, *3*. https://doi.org/10.7554/elife.02077

Barghi, N., Tobler, R., Nolte, V., Jakšić, A. M., Mallard, F., Otte, K. A., Dolezal, M., Taus, T., Kofler, R., & Schlötterer, C. (2019). Genetic redundancy fuels polygenic adaptation in Drosophila. *PLoS Biology*, *17*(2). https://doi.org/10.1371/journal.pbio.3000128

Barter, T. T., Greenspan, Z. S., Phillips, M. A., Mueller, L. D., Rose, M. R., & Ranz, J. M. (2019). Drosophila transcriptomics with and without ageing. *Biogerontology*, *20*(5). https://doi.org/10.1007/s10522-019-09823-4

Bates, D., Mächler, M., Bolker, B. M., & Walker, S. C. (2015). Fitting linear mixed-effects models using lme4. *Journal of Statistical Software*, *67*(1). https://doi.org/10.18637/jss.v067.i01

Benjamini, Y., & Hochberg, Y. (1995). Controlling the False Discovery Rate: A Practical and Powerful Approach to Multiple Testing. *Journal of the Royal Statistical Society: Series B (Methodological)*, *57*(1). https://doi.org/10.1111/j.2517-6161.1995.tb02031.x

Bujak, R., Daghir-Wojtkowiak, E., Kaliszan, R., & Markuszewski, M. J. (2016). PLS-based and regularization-based methods for the selection of relevant variables in non-targeted metabolomics data. *Frontiers in Molecular Biosciences*, *3*(JUL). https://doi.org/10.3389/fmolb.2016.00035

Burke, M. K., Barter, T. T., Cabral, L. G., Kezos, J. N., Phillips, M. A., Rutledge, G. A., Phung, K. H., Chen, R. H., Nguyen, H. D., Mueller, L. D., & Rose, M. R. (2016). Rapid divergence and convergence of life-history in experimentally evolved Drosophila melanogaster. *Evolution; International Journal of Organic Evolution*, *70*(9). https://doi.org/10.1111/evo.13006

Burke, M. K., Dunham, J. P., Shahrestani, P., Thornton, K. R., Rose, M. R., & Long, A. D. (2010). Genome-wide analysis of a long-term evolution experiment with Drosophila. *Nature*, *467*(7315). https://doi.org/10.1038/nature09352

Carnes, M. U., Campbell, T., Huang, W., Butler, D. G., Carbone, M. A., Duncan, L. H., Harbajan, S. v., King, E. M., Peterson, K. R., Weitzel, A., Zhou, S., & Mackay, T. F. C. (2015). The genomic basis of postponed senescence in Drosophila melanogaster. *PLoS ONE*, *10*(9). https://doi.org/10.1371/journal.pone.0138569

Cavigliasso, F., Savary, L., Spangenberg, J. E., Gallart-Ayala, H., Ivanisevic, J., & Kawecki, T. J. (2023). Experimental evolution of metabolism under nutrient restriction: enhanced amino acid catabolism and a key role of branched-chain amino acids. *Evolution Letters*, *7*(4). https://doi.org/10.1093/evlett/qrad018

Chaleckis, R., Murakami, I., Takada, J., Kondoh, H., & Yanagida, M. (2016). Individual variability in human blood Metabolites identifies age-related differences. *Proceedings of the National Academy of Sciences of the United States of America*, *113*(16). https://doi.org/10.1073/pnas.1603023113

Charlesworth, B. (1980). Evolution in age-structured populations. *Evolution in Age-Structured Populations.* https://doi.org/10.2307/4092

Chippindale, A. K., Alipaz, J. A., Chen, H. W., & Rose, M. R. (1997). Experimental evolution of accelerated development in Drosophila. 1. Developmental speed and larval survival. *Evolution*, *51*(5). https://doi.org/10.1111/j.1558-5646.1997.tb01477.x

Conway, J. R., Lex, A., & Gehlenborg, N. (2017). UpSetR: An R package for the visualization of intersecting sets and their properties. *Bioinformatics*, *33*(18). https://doi.org/10.1093/bioinformatics/btx364

Dettmer, K., Aronov, P. A., & Hammock, B. D. (2007). Mass spectrometry-based metabolomics. In *Mass Spectrometry Reviews* (Vol. 26, Issue 1). https://doi.org/10.1002/mas.20108

Dittmann, A., Kennedy, N. J., Soltero, N. L., Morshed, N., Mana, M. D., Yilmaz, Ö. H., Davis, R. J., & White, F. M. (2019). High-fat diet in a mouse insulin-resistant model induces widespread rewiring of the phosphotyrosine signaling network. *Molecular Systems Biology*, *15*(8). https://doi.org/10.15252/msb.20198849

Elmansi, A. M., Hussein, K. A., Herrero, S. M., Periyasamy-Thandavan, S., Aguilar-Pérez, A., Kondrikova, G., Kondrikov, D., Eisa, N. H., Pierce, J. L., Kaiser, H., Ding, K. H., Walker, A. L., Jiang, X., Bollag, W. B., Elsalanty, M., Zhong, Q., Shi, X. ming, Su, Y., Johnson, M., … Hill, W. D. (2020). Age-related increase of kynurenine enhances miR29b-1-5p to decrease both

CXCL12 signaling and the epigenetic enzyme Hdac3 in bone marrow stromal cells. *Bone Reports*, *12*. https://doi.org/10.1016/j.bonr.2020.100270

Fabian, D. K., Garschall, K., Klepsatel, P., Santos-Matos, G., Sucena, É., Kapun, M., Lemaitre, B., Schlötterer, C., Arking, R., & Flatt, T. (2018). Evolution of longevity improves immunity in Drosophila. In *Evolution Letters* (Vol. 2, Issue 6). https://doi.org/10.1002/evl3.89

Friedman, J., Hastie, T., Tibshirani, R., Balasubramanian Narasimhan, Kenneth Tay, Noah Simon, Junyang Qian, & James Yang. (2023). Package 'glmnet' - Lasso and Elastic-Net Regularized Generalized Linear Models. In *CRAN*.

Ge, I., Kirschen, G. W., & Wang, X. (2021). Shifted Dynamics of Glucose Metabolism in the Hippocampus During Aging. *Frontiers in Aging Neuroscience*, *13*. https://doi.org/10.3389/fnagi.2021.700306

Graves, J. L., Hertweck, K. L., Phillips, M. A., Han, M. v., Cabral, L. G., Barter, T. T., Greer, L. F., Burke, M. K., Mueller, L. D., Rose, M. R., & Singh, N. (2017). Genomics of parallel experimental evolution in drosophila. *Molecular Biology and Evolution*, *34*(4). https://doi.org/10.1093/molbev/msw282

Greenspan, Z., Barter, T., Phillips, M., Ranz, J., Rose, M., & Mueller, L. (2024). Genomewide architecture of adaptation in experimentally evolved Drosophila characterized by widespread pleiotropy. *Journal of Genetics* , *103*(1), 8.

Han, X., Liu, C., Xue, Y., Wang, J., Xue, C., Yanagita, T., Gao, X., & Wang, Y. (2016). Long-term fatty liver-induced insulin resistance in orotic acid-induced nonalcoholic fatty liver rats. *Bioscience, Biotechnology and Biochemistry*, *80*(4). https://doi.org/10.1080/09168451.2015.1123608

Hardy, C. M., Burke, M. K., Everett, L. J., Han, M. v., Lantz, K. M., & Gibbs, A. G. (2018). Genome-Wide Analysis of Starvation-Selected Drosophila melanogaster-A Genetic Model of Obesity. *Molecular Biology and Evolution*, *35*(1). https://doi.org/10.1093/molbev/msx254

Harrison, B. R., Wang, L., Gajda, E., Hoffman, E. v., Chung, B. Y., Pletcher, S. D., Raftery, D., & Promislow, D. E. L. (2020). The metabolome as a link in the genotype-phenotype map for peroxide resistance in the fruit fly, Drosophila melanogaster. *BMC Genomics*, *21*(1). https://doi.org/10.1186/s12864-020-6739-1

Hoffman, J. M., Soltow, Q. A., Li, S., Sidik, A., Jones, D. P., & Promislow, D. E. L. (2014). Effects of age, sex, and genotype on high-sensitivity metabolomic profiles in the fruit fly, Drosophila melanogaster. *Aging Cell*, *13*(4). https://doi.org/10.1111/acel.12215

Houtkooper, R. H., Argmann, C., Houten, S. M., Canńo, C., Jeninga, E. H., Andreux, Ṕeńelope A., Thomas, C., Doenlen, R., Schoonjans, K., & Auwerx, J. (2011). The metabolic footprint of aging in mice. *Scientific Reports*, *1*. https://doi.org/10.1038/srep00134

Inouye, M., Mio, T., & Sumino, K. (2000). Dicarboxylic acids as markers of fatty acid peroxidation in diabetes. *Atherosclerosis*, *148*(1). https://doi.org/10.1016/S0021-9150(99)00263-4

Ives, P. T. (1970). Further Genetic Studies of the South Amherst Population of Drosophila melanogaster. *Evolution*, *24*(3). https://doi.org/10.2307/2406830

Jin, K., Wilson, K. A., Beck, J. N., Nelson, C. S., Brownridge, G. W. G. W., Harrison, B. R., Djukovic, D., Raftery, D., Brem, R. B., Yu, S., Drton, M., Shojaie, A., Kapahi, P., & Promislow, D. (2020). Genetic and metabolomic architecture of variation in diet restriction-mediated lifespan extension in Drosophila. *PLoS Genetics*, *16*(7). https://doi.org/10.1371/journal.pgen.1008835

Jylhävä, J., Pedersen, N. L., & Hägg, S. (2017). Biological Age Predictors. In *EBioMedicine* (Vol. 21). https://doi.org/10.1016/j.ebiom.2017.03.046

Kezos, J. N., Barter, T. T., Phillips, M. A., Cabral, L. G., Greenspan, Z. S., Arnold, K. R., Azatian, G., Buenrostro, J., Bhangoo, P. S., Khong, A., Reyes, G. T., Rahman, A., Humphrey, L. A., Bradley, T. J., Mueller, L. D., & Rose, M. R. (2023). Building Bridges from Genome to Physiology Using Machine Learning and Drosophila Experimental Evolution. *Physiological and Biochemical Zoology*, *96*(3). https://doi.org/10.1086/724827

Kezos, J. N., Phillips, M. A., Thomas, M. D., Ewunkem, A. J., Rutledge, G. A., Barter, T. T., Santos, M. A., Wong, B. D., Arnold, K. R., Humphrey, L. A., Yan, A., Nouzille, C., Sanchez, I., Cabral, L. G., Bradley, T. J., Mueller, L. D., Graves, J. L., & Rose, M. R. (2019). Genomics of Early Cardiac Dysfunction and Mortality in Obese Drosophila melanogaster. *Physiological and Biochemical Zoology : PBZ*, *92*(6). https://doi.org/10.1086/706099

Kim, D. K., Jeon, H., & Cha, D. S. (2014). 4-Hydroxybenzoic acid-mediated lifespan extension in Caenorhabditis elegans. *Journal of Functional Foods*, *7*(1). https://doi.org/10.1016/j.jff.2013.12.022

Kolde, R. (2022). Package “pheatmap”: Pretty heatmaps. *R Package*.

Koliada, A., Gavrilyuk, K., Burdylyuk, N., Strilbytska, O., Storey, K. B., Kuharskii, V., Lushchak, O., & Vaiserman, A. (2020). Mating status affects Drosophila lifespan, metabolism and antioxidant system. *Comparative Biochemistry and Physiology -Part A : Molecular and Integrative Physiology*, *246*. https://doi.org/10.1016/j.cbpa.2020.110716

Kozieł, K., & Urbanska, E. M. (2023). Kynurenine Pathway in Diabetes Mellitus—Novel Pharmacological Target? In *Cells* (Vol. 12, Issue 3). https://doi.org/10.3390/cells12030460

Kurup, K., Matyi, S., Giles, C. B., Wren, J. D., Jones, K., Ericsson, A., Raftery, D., Wang, L., Promislow, D., Richardson, A., & Unnikrishnan, A. (2021). Calorie restriction prevents age-related changes in the intestinal microbiota. *Aging*, *13*(5). https://doi.org/10.18632/aging.202753

Kvalseth, T. O. (1985). Cautionary note about r2. *American Statistician*, *39*(4). https://doi.org/10.1080/00031305.1985.10479448

Lassen, J. K., Wang, T., Nielsen, K. L., Hasselstrøm, J. B., Johannsen, M., & Villesen, P. (2023). Large-Scale metabolomics: Predicting biological age using 10,133 routine untargeted LC–MS measurements. *Aging Cell*, *22*(5). https://doi.org/10.1111/acel.13813

Laye, M. J., Tran, V., Jones, D. P., Kapahi, P., & Promislow, D. E. L. (2015). The effects of age and dietary restriction on the tissue-specific metabolome of Drosophila. *Aging Cell*, *14*(5). https://doi.org/10.1111/acel.12358

Liang, Y., Dai, X., Cao, Y., Wang, X., Lu, J., Xie, L., Liu, K., & Li, X. (2023). The neuroprotective and antidiabetic effects of trigonelline: A review of signaling pathways and molecular mechanisms. In *Biochimie* (Vol. 206). https://doi.org/10.1016/j.biochi.2022.10.009

Lu, A. T., Fei, Z., Haghani, A., Robeck, T. R., Zoller, J. A., Li, C. Z., Lowe, R., Yan, Q., Zhang, J., Vu, H., Ablaeva, J., Acosta-Rodriguez, V. A., Adams, D. M., Almunia, J., Aloysius, A., Ardehali, R., Arneson, A., Baker, C. S., Banks, G., … Horvath, S. (2023). Universal DNA methylation age across mammalian tissues. *Nature Aging*, *3*(9). https://doi.org/10.1038/s43587-023-00462-6

Luckinbill, L. S., Arking, R., Clare, M. J., Cirocco, W. C., & Buck, S. A. (1984). Selection for Delayed Senescence in Drosophila melanogaster. *Evolution*, *38*(5). https://doi.org/10.2307/2408433

Maslov, D. L., Zemskaya, N. v., Trifonova, O. P., Lichtenberg, S., Balashova, E. E., Lisitsa, A. v., Moskalev, A. A., & Lokhov, P. G. (2021). Comparative metabolomic study of drosophila species with different lifespans. *International Journal of Molecular Sciences*, *22*(23). https://doi.org/10.3390/ijms222312873

Meador, J. P., Bettcher, L. F., Ellenberger, M. C., & Senn, T. D. (2020). Metabolomic profiling for juvenile Chinook salmon exposed to contaminants of emerging concern. *Science of the Total Environment*, *747*. https://doi.org/10.1016/j.scitotenv.2020.141097

Meyer, D. H., & Schumacher, B. (2024). Aging clocks based on accumulating stochastic variation. *Nature Aging*. https://doi.org/10.1038/s43587-024-00619-x

Navas-Enamorado, C., Capo, X., Galmes-Panades, A. M., Ortega-Moral, A., Sánchez-Polo, A., Masmiquel, L., Torrens-Mas, M., Navas, P., & Gonzalez-Freire, M. (2024). The association of circulating bioenergetic metabolites with healthy human aging. *Experimental Gerontology*, *194*, 112488. https://doi.org/10.1016/j.exger.2024.112488

Palomino-Schätzlein, M., Simó, R., Hernández, C., Ciudin, A., Mateos-Gregorio, P., Hernández-Mijares, A., Pineda-Lucena, A., & Herance, J. R. (2018). Metabolic fingerprint of insulin resistance in human polymorphonuclear leucocytes. *PLoS ONE*, *13*(7). https://doi.org/10.1371/journal.pone.0199351

Parrott, B. B., & Bertucci, E. M. (2019). Epigenetic Aging Clocks in Ecology and Evolution. In *Trends in Ecology and Evolution* (Vol. 34, Issue 9). https://doi.org/10.1016/j.tree.2019.06.008

Patti, G. J., Yanes, O., & Siuzdak, G. (2012). Innovation: Metabolomics: the apogee of the omics trilogy. In *Nature Reviews Molecular Cell Biology* (Vol. 13, Issue 4). https://doi.org/10.1038/nrm3314

Phillips, M. A., Arnold, K. R., Vue, Z., Beasley, H. K., Garza-Lopez, E., Marshall, A. G., Morton, D. J., McReynolds, M. R., Barter, T. T., & Hinton, A. (2022). Combining Metabolomics and Experimental Evolution Reveals Key Mechanisms Underlying Longevity Differences in Laboratory Evolved Drosophila melanogaster Populations. *International Journal of Molecular Sciences*, *23*(3). https://doi.org/10.3390/ijms23031067

Phillips, M. A., Long, A. D., Greenspan, Z. S., Greer, L. F., Burke, M. K., Villeponteau, B., Matsagas, K. C., Rizza, C. L., Mueller, L. D., & Rose, M. R. (2016). Genome-wide analysis of long-term evolutionary domestication in Drosophila melanogaster. *Scientific Reports*, *6*. https://doi.org/10.1038/srep39281

Rodrigues, M. A., Dauphin-Villemant, C., Paris, M., Kapun, M., Mitchell, E. D., Kerdaffrec, E., & Flatt, T. (2023). Germline proliferation trades off with lipid metabolism in *Drosophila*. *Evolution Letters*. https://doi.org/10.1093/evlett/qrad059

Rose, M., & Charlesworth, B. (1980). A test of evolutionary theories of senescence. *Nature*, *287*(5778). https://doi.org/10.1038/287141a0

Rose, M., Passananti, H., & Matos, M. (2010). Methuselah Flies - A Case Study in the Evolution of Aging. In *Methuselah Flies - A Case Study in the Evolution of Aging*. https://doi.org/10.1142/9789812567222

Rose, M. R. (1984). Laboratory Evolution of Postponed Senescence in Drosophila melanogaster. *Evolution*, *38*(5). https://doi.org/10.2307/2408434

Rose, M. R., & Charlesworth, B. (1981). Genetics of life history in Drosophila melanogaster. II. Exploratory selection experiments. *Genetics*, *97*(1). https://doi.org/10.1093/genetics/97.1.187

Rose, M. R., Rauser, C. L., Benford, G., Matos, M., & Mueller, L. D. (2007). Hamilton's forces of natural selection after forty years. In *Evolution* (Vol. 61, Issue 6). https://doi.org/10.1111/j.1558-5646.2007.00120.x

Rutledge, J., Oh, H., & Wyss-Coray, T. (2022). Measuring biological age using omics data. In *Nature Reviews Genetics* (Vol. 23, Issue 12). https://doi.org/10.1038/s41576-022-00511-7

Son, N., Hur, H. J., Sung, M. J., Kim, M. S., Hwang, J. T., Park, J. H., Yang, H. J., Kwon, D. Y., Yoon, S. H., Chung, H. Y., & Kim, H. J. (2012). Liquid chromatography-mass spectrometry-based metabolomic analysis of livers from aged rats. *Journal of Proteome Research*, *11*(4). https://doi.org/10.1021/pr201263q

Team, R. C. (2023). R Core Team 2023 R: A language and environment for statistical computing. R foundation for statistical computing. https://www.R-project.org/. *R Foundation for Statistical Computing*.

Tobler, R., Hermisson, J., & Schlötterer, C. (2015). Parallel trait adaptation across opposing thermal environments in experimental Drosophila melanogaster populations. *Evolution*, *69*(7). https://doi.org/10.1111/evo.12705

Turner, T. L., Stewart, A. D., Fields, A. T., Rice, W. R., & Tarone, A. M. (2011). Population-based resequencing of experimentally evolved populations reveals the genetic basis of body size

variation in Drosophila melanogaster. *PLoS Genetics*, *7*(3). https://doi.org/10.1371/journal.pgen.1001336

Wang, Y., Grenell, A., Zhong, F., Yam, M., Hauer, A., Gregor, E., Zhu, S., Lohner, D., Zhu, J., & Du, J. (2018). Metabolic signature of the aging eye in mice. *Neurobiology of Aging*, *71*. https://doi.org/10.1016/j.neurobiolaging.2018.07.024

Wickham, H. (2016). ggplot2 Elegant Graphics for Data Analysis (Use R!). *Springer*.

Xiang, L., Nie, J., Wang, L., Wang, Y., Shi, J., Wei, J., Lau, C. W., Cai, Z., & Huang, Y. (2021). Integrated metabolomics analysis of the effect of PPARδ agonist GW501516 on catabolism of BCAAs and carboxylic acids in diabetic mice. *Chinese Chemical Letters*, *32*(7). https://doi.org/10.1016/j.cclet.2020.12.042

Yamauchi, T., Oi, A., Kosakamoto, H., Akuzawa-Tokita, Y., Murakami, T., Mori, H., Miura, M., & Obata, F. (2020). Gut Bacterial Species Distinctively Impact Host Purine Metabolites during Aging in Drosophila. *IScience*, *23*(9). https://doi.org/10.1016/j.isci.2020.101477

Yang, Y., Huang, Z., Yang, Z., Qi, Y., Shi, H., Zhou, Y., Wang, F., & Yang, M. (2021). Serum metabolomic profiling reveals an increase in homocitrulline in Chinese patients with nonalcoholic fatty liver disease: A retrospective study. *PeerJ*, *9*. https://doi.org/10.7717/peerj.11346

Zeng, W. Y., Tan, L., Han, C., Zheng, Z. Y., Wu, G. S., Luo, H. R., & Li, S. L. (2021). Trigonelline Extends the Lifespan of C. Elegans and Delays the Progression of Age-Related Diseases by Activating AMPK, DAF-16, and HSF-1. *Oxidative Medicine and Cellular Longevity*, *2021*. https://doi.org/10.1155/2021/7656834

Zhao, X., Golic, F. T., Harrison, B. R., Manoj, M., Hoffman, E. v., Simon, N., Johnson, R., MacCoss, M. J., McIntyre, L. M., & Promislow, D. E. L. (2022). The metabolome as a biomarker of aging in Drosophila melanogaster. *Aging Cell*, *21*(2). https://doi.org/10.1111/acel.13548

Zhuang, H., Karvinen, S., Törmäkangas, T., Zhang, X., Ojanen, X., Velagapudi, V., Alen, M., Britton, S. L., Koch, L. G., Kainulainen, H., Cheng, S., & Wiklund, P. (2021). Interactive effects of aging and aerobic capacity on energy metabolism–related metabolites of serum, skeletal muscle, and white adipose tissue. *GeroScience*, *43*(6). https://doi.org/10.1007/s11357-021-00387-1

Zou, H., & Hastie, T. (2005). Regularization and variable selection via the elastic net. *Journal of the Royal Statistical Society. Series B: Statistical Methodology*, *67*(2). https://doi.org/10.1111/j.1467-9868.2005.00503.x